

# Sterile neutrino searches with reactor antineutrinos using coherent neutrino-nucleus scattering experiments

S.P. Behera<sup>1,\*</sup>, D.K. Mishra<sup>1</sup>, P.K. Netrakanti<sup>1</sup>, R. Sehgal<sup>1</sup>, Kirtikesh Kumar<sup>1</sup>, R. Dey<sup>1,2</sup>, and V. Jha<sup>1,2</sup>

<sup>1</sup>*Nuclear Physics Division, Bhabha Atomic Research Centre,  
Mumbai - 400085, India and*

<sup>2</sup>*Homi Bhabha National Institute, Anushakti Nagar, Mumbai - 400094, India*

We present an analysis on the sensitivity to the active-sterile neutrino mixing with Germanium (Ge) and Silicon (Si) detectors in the context of the proposed coherent elastic neutrino-nucleus experiment in India. The study has been carried out with 3 (active) + 1 (sterile) neutrino oscillation model. It is observed that the measurements that can be carried out with the Ge detector exhibit better sensitivity to the active-sterile neutrino mixing as compared to the Si detector. Both detectors are able to exclude most of the anomaly regions observed by the GALLIUM experiment. The Ge detector with mass 10 kg, can observe the active-sterile neutrino oscillation at 95% confidence level, provided that  $\sin^2 2\theta_{14} \geq 0.09$  at  $\Delta m_{41}^2 = 1.0 \text{ eV}^2$  for an exposure of 1-yr. At higher values of  $\Delta m_{41}^2$ , a better sensitivity is obtained at a short baseline. It is also found that the threshold as well as resolution of the detectors play a crucial role on the measurements of active-sterile neutrino mixing parameters.

## I. INTRODUCTION

The concept of neutrino was first introduced by Pauli in 1930 while explaining the energy spectra of beta particles. Later on, it was first observed by Cowan and Reines via the inverse beta decay (IBD) process using the reactor as a source. The small mass of neutrinos results from the combination of three mass eigen-states, which is established by many experiments using solar, atmospheric, reactor, and accelerator-based neutrinos. However, the physical origin of their masses is still not understood. Since, neutrinos do not have fixed mass but are described by quantum mechanical superposition mass eigen-states ( $\nu_1, \nu_2, \nu_3$ ), with each one having distinct mass eigen-value  $m_1, m_2, m_3$ . Neutrinos can change flavor while moving from one place to another, a phenomenon commonly referred to as neutrino flavor oscillation. At present several efforts are going on for the precise determination of neutrino oscillation parameters [1, 2]. Many experiments are being performed to obtain more accurate values of neutrino-nucleus cross-sections. Coherent elastic neutrino-nucleus scattering (CE $\nu$ NS) is a standard model (SM) process where the low energy neutrinos scatter off the atomic nucleus coherently through the neutral-current weak interactions [3]. For low-energy neutrinos ( $< 50 \text{ MeV}$ ), the CE $\nu$ NS process has a larger cross-section for neutron-rich targets compared to other known processes, such as inverse beta decay (IBD) and neutrino-electron scattering [4], which have been traditionally used for neutrino measurements. Further, the CE $\nu$ NS is a threshold-less process in contrast to IBD. Although, having a larger cross-section, the CE $\nu$ NS process has not been observed earlier due to the challenge of measuring the low-energy recoil nuclei. The measurement of CE $\nu$ NS cross-section requires a high flux of low energy neutrinos and measurement of low nuclear recoil energies.

There are mainly three possible sources of (anti)neutrinos

that could be used to search for the measurement of the CE $\nu$ NS process, namely pion decay at rest (DAR) beam, an intense radioactive source, or a nuclear reactor. Recently, the CE $\nu$ NS cross-section has been measured by the COHERENT experiment using the neutrinos produced from the spallation neutron source as a DAR [5]. The neutrinos produced due to this method have a maximum energy of about 53 MeV. The endeavor to measure CE $\nu$ NS using neutrinos from a nuclear reactor or an intense radioactive source presents both challenges and intriguing possibilities. In the case of reactor,  $\bar{\nu}_e$ s produced due to nuclear fission have an endpoint energy near 10 MeV. Due to the lower neutrino energies as compared to other sources, it becomes imperative to employ novel detector technologies capable of achieving detection thresholds in the range of a few tens of eV. Various cryogenic bolometers stand out as promising candidates for optimization to meet this need.

The measurement of CE $\nu$ NS cross-section by the COHERENT group has opened up an avenue for exploring various aspects related to physics beyond the SM at low energy. At present, several experiments are going on and some are proposed to measure the CE $\nu$ NS cross-section with the required threshold by using charge-coupled devices (CCDs), metallic superconducting bolometers, Ge-based semiconductor detectors, and the Scintillating Bubble Chamber [6] employing reactor  $\bar{\nu}_e$  as a source [4, 7–13]. The measurement of the CE $\nu$ NS process can shed light on several fundamental SM physics aspects such as non-standard interactions [14, 15], neutron density distribution [16], neutrino magnetic moment [17], and the weak mixing angle [18, 19]. The CE $\nu$ NS is a flavor-blind process, hence flavor-independent astronomy with supernova neutrinos becomes feasible, which allows us to investigate the interior of dense objects as well as stellar evolution in details [20, 21].

In this context, we propose to measure the CE $\nu$ NS process using the reactor  $\bar{\nu}_e$ s in India, to address various fundamental physics aspects of neutrino as mentioned earlier. The present study focused on investigating the possible explanation for an anomalous behavior found in several SBL reactor exper-

---

\*Electronic address: [shiba@barc.gov.in](mailto:shiba@barc.gov.in)

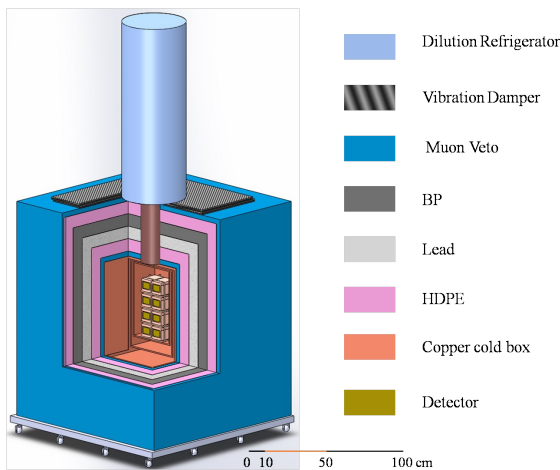


FIG. 1: Schematic representation of experimental setup for  $\text{CE}\nu\text{NS}$  measurement. BP: boronated polyethylene, thickness: 10 cm, HDPE: high density polyethylene, thickness: 10 cm

iments that measure the  $\bar{\nu}_e$ s through the IBD process [22]. The precise recalculation of the  $\bar{\nu}_e$  flux by Mueller *et al.* [23] and Huber [24] shows about 6% deficit in the observed-to-predicted ratio of events at a short distance through the IBD process, which is known as the “reactor antineutrino anomaly” (RAA) [22]. There are two distinct explanations proposed for this discrepancy. One of them is the disappearance of  $\bar{\nu}_e$  while propagating from the source to detector due to Active-Sterile Neutrino (ASN) oscillations with the mass square difference  $\Delta m^2 \sim 1 \text{ eV}^2$ . On the other hand, the observed discrepancy is likely to be related to the inaccuracies in predicting antineutrino flux, stemming from incomplete reactor models or uncertainties in nuclear data. The Huber-Muller model utilizes the cumulative  $\beta^-$ -spectra measured at ILL for conversion to antineutrino spectra [23, 24]. This suggests that experimental biases, possibly related to these measurements, might account for the anomaly. Recent measurements indicate that bias in the prediction of  $^{235}\text{U}$  flux may be the likely cause of RAA [25, 26]. The  $\text{CE}\nu\text{NS}$  process has an advantage compared to other techniques for finding the possible existence of the sterile neutrino. It is a neutral current process in which neutrinos scatter off the nuclei, and are independent of the neutrino flavor. Therefore, any finding of an oscillation structure would signify complete mixing with non-active neutrinos.

Recently, various experiments have carried out the reactor  $\bar{\nu}_e$ s measurement to study the ASN oscillations using the IBD process. The DANSS collaboration has measured the positron energy spectra at 3 different distances (ranging from 10.7 m to 12 m) from the reactor core. From the measurements, a large fraction of the RAA region in the  $\sin^2 2\theta_{14} - \Delta m_{41}^2$  plane that covers the parameter space up to  $\sin^2 2\theta_{14} < 0.01$  [27] are excluded. Similarly, the STEREO [28] collaboration has measured the  $\bar{\nu}_e$  energy spectrum in six different detector cells covering baselines between 9 and 11 meters from the reactor core of the ILL research reactor. The results based on the current reactor ON data are explained by the null ASN oscillation hypothesis and the best fit of the RAA can be ex-

cluded at 97.5% confidence level (C.L.). The reactor  $\bar{\nu}_e$  spectra measured by PROSPECT collaboration disfavors the RAA best-fit point at  $2.2\sigma$  C.L. and constrains significant portions of the previously allowed parameter space at 95% C.L.[29]. The Neutrino-4 group has measured  $\bar{\nu}_e$  energy spectra with the segmented detectors at different positions ranging from 6 to 12 meters. Their model-independent analysis excludes the RAA region at C.L. more than  $3\sigma$ . However, the experiment has observed ASN oscillation at  $\sin^2 2\theta_{14} = 0.39$  and  $\Delta m_{41}^2 = 7.3 \text{ eV}^2$  at C.L. of  $2.8\sigma$  [30]. The above experimental observations are found by detecting  $\bar{\nu}_e$  through the IBD process. There are several experiments currently proposed or planned to investigate the mixing of active-sterile neutrinos using  $\text{CE}\nu\text{NS}$  process [8, 31]. In pursuit of this goal, a feasibility study has been carried out to ascertain the ASN mixing sensitivity of various types of detectors by placing them at a short baseline ( $L \leq 30\text{m}$ ) through  $\text{CE}\nu\text{NS}$  channel.

The article is organized as follows. In the subsequent section, a comprehensive description of the detector setup is provided. Antineutrinos production and various types of reactors used in this study are presented in Sec.III. The  $\text{CE}\nu\text{NS}$  process and the underlying detection principle are expounded upon in Sec. IV. An estimation of the expected number of events in the detector is presented in Section V. The phenomenon of ASN oscillation at short baseline considering the ‘3+1’ mixing model is described in Sec. VI. The simulation procedure for incorporation of detector response on coherent neutrino discussed in Sec. VII. The sensitivity of the proposed experiment, statistical method on  $\chi^2$  estimation considered in this study is discussed in Sec. VIII. The sensitivity to sterile neutrino mixing at an exposure of one year is elaborated in Sec. IX. Finally, in Sec. X, we summarize our observations and discuss the implication of this work.

## II. DETECTOR SETUP AT $\text{CE}\nu\text{NS}$ MEASUREMENT

Figure 1 shows the conceptual schematic of the detector setup proposed for the measurement of  $\text{CE}\nu\text{NS}$  using antineutrinos produced from the reactor. The core detector volume is covered with various shielding materials for reducing backgrounds. The active volume of the detector is placed at the center within a cold copper box that is surrounded by 4 cm thick plastic scintillator plates for vetoing cosmic muon. High-density polyethylene(HDPE) sheets of thickness 10 cm are placed next to the muon veto detectors for thermalizing the fast neutrons. A Lead shielding of 10 cm thickness is added to reduce the natural and reactor-generated gamma-rays background. Boronated polyethylene (BP) sheets with 15% boron content and thickness of 10 cm are positioned at the outer part of the setup to attenuate the thermal neutrons. The thickness of Lead and BP sheets are chosen considering the previous study performed for another reactor-based antineutrino experiment using the ISMRAN detector [32]. To maintain the required low temperature for detector operation, dilution refrigerator atop a vibration damper is placed on the outer layer of the shielding. A link is established by a cold finger arrangement of length 50 cm between the refrigerator and detector, to

TABLE I: Reactor details

Reactors name	Thermal power( $MW_{th}$ )	Fuel type
U-Apsara	3.0	$U_3Si_2$ -Al (17% enriched $^{235}U$ )
DHRUVA	100.0	Natural uranium (0.7% $^{235}U$ )
PFBR	1250.0	MOX( $PuO_2$ - $UO_2$ )
VVER	3000.0	$UO_2$ (3.92 % enriched $^{235}U$ )

maintain the temperature stability in the active volume. The detectors will be housed within a copper-cooled box of dimension  $50 \times 50 \times 75 \text{ cm}^3$ , with a 2 cm thick copper plate. The proposed detector will be placed at 4m distance from the movable U-Apsara reactor core in the designated area within the reactor hall.

The incoming particle energy can be determined from particle interactions in a target which includes the measurement of ionization, scintillation, and/or the phonon excitation in the material. The ionization signal is generated as the electron-hole pairs, which are produced during the energy loss process and collected on the electrodes. The metal electrodes on the two faces of the crystal substrate acting as sensors to measure ionization. Simultaneously, a thermal sensor in contact with the Si/Ge crystal records the phonon signal, similar to the one discussed in [33]. Currently, two types of detectors such as high-purity Si or Ge are under consideration for measuring the signal produced by recoil nuclei. Each crystal is equipped with two concentric ionization electrodes, and four independent phonon sensors are photolithographically patterned. The phonon signal is measured using the Transition edge sensor (TES) sensor [10]. Our proposed detector aims to measure both the ionization and phonon energy for every event, enabling the simultaneous measurement of both signals. This combined information offers an efficient discrimination against the significant background of electron recoils originating from the natural  $\gamma$  and  $\beta$  radioactivity. Additionally, the ionization signal can be combined with the phonon signal to provide the true energy of the nuclear recoil and for the deduction of quenching factor,  $Q$  [34].

### III. ANTI-NEUTRINOS FROM NUCLEAR REACTOR

A nuclear reactor is an intense source of electron  $\bar{\nu}_e$ s. There are two primary processes contribute to the generation of  $\bar{\nu}_e$ s within the reactor. One of them is the beta decay of fission fragments, predominantly from four isotopes  $^{235}U$ ,  $^{238}U$ ,  $^{239}Pu$  and  $^{241}Pu$  and the second one is the neutron capture process on  $^{238}U$ . The antineutrinos produced from the beta decay of fission fragments have energy up to about 10 MeV, while those produced from neutron capture have energy less than 2 MeV. There are on an average six  $\bar{\nu}_e$ s produced per fission excluding  $\bar{\nu}_e$ s produced due to neutron capture. Reactor  $\bar{\nu}_e$ s with energy greater than 2.0 MeV are easy to detect, whereas measuring low-energy  $\bar{\nu}_e$ s poses a significant challenge [35]. In the present work, we have considered the full neutrino flux that includes contribution from fission as well as neutron capture ( $^{238}U(n, \gamma)^{239}U$ ) process. The parameteriza-

tion for  $\bar{\nu}_e$ s energy spectra above 2.0 MeV is considered from the Huber-Muller model [23, 24]. The low energy  $\bar{\nu}_e$ s flux distribution due to fission  $^{235}U$ ,  $^{238}U$ ,  $^{239}Pu$  and  $^{241}Pu$  is considered from Ref. [36] and the neutron capture process on the  $^{238}U$  taken from Ref. [37]. The relative contribution of each isotope depends on the type of reactor and its fuel cycle. In this study, reactors with different core compositions are considered as discussed below. In the beginning, it is planned to perform measurements with the detector at 4 m from the reactor core in the upgraded Apsara (U-Apsara) research reactor facility in Bhabha Atomic Research Centre (BARC), India. The U-Apsara reactor has a compact core with a height of about 0.64 m and a radius of about 0.32 m which can operate at a maximum thermal power of 3  $MW_{th}$  [38]. The main advantage of the U-Apsara reactor is that its core is movable so the measurement can be performed at different baselines which leads to canceling the reactor as well as detector related systematic uncertainties. In future, the same detector setup can be placed at other reactor facilities such as DHRUVA, BARC [39], Proto-type Fast Breeder Reactor (PFBR), IG-CAR, Kalpakkam, and VVER, Kudankulam in India [40]. The DHRUVA reactor core has radius  $\sim 1.5$  m and height  $\sim 3.03$  m (defined as an extended source) [39], which can operate at a maximum thermal power of 100  $MW_{th}$  consuming natural uranium as fuel. On the other hand, PFBR is relatively a compact source as compared to DHRUVA with a dimension of about 1 m both in radius and height. The PFBR can operate at a maximum thermal power of 1250  $MW_{th}$  with mixed oxide (MOX,  $PuO_2$ - $UO_2$ ) as fuel [40]. The VVER power reactor has thermal power of 3000  $MW_{th}$  and core has radius  $\sim 1.5$  m and height  $\sim 3.03$  m (also an extended source). The VVER reactor is a pressurized water reactor and uses 3.92% enriched uranium as a fuel [41]. It can be noted here that the fractional contributions of each isotope to the reactor thermal power and the parameter lists used to fit the neutrino energy spectra for the above mentioned reactor are mentioned in Ref. [42]. Due to their compact size, U-Apsara and PFBR reactors are the ideal sources to utilize the detector set-up for investigating the ASN mixing at short distances. On the other hand, at very close distances there are significant background contributions from the reactor come into play, impacting the sensitivity of sterile neutrino measurements. The above-mentioned reactors are not only different with respect to their sizes and thermal power but also in fuel compositions, as detailed in Table I.

#### IV. COHERENT NEUTRINO-NUCLEUS SCATTERING MEASUREMENT

The CE $\nu$ NS scattering has been first proposed by Freedman [3] within the SM. In this process, the low-energy neutrinos scatter off nuclei which carry only energies up to a few keV. It is very hard to measure such low energies ( $\sim$  few tens of eV) of recoiling nuclei which requires the minimization of uncertainties associated with the relevant measurements. The differential CE $\nu$ NS scattering cross-section is expressed as:

$$\frac{d\sigma}{dT}(E_\nu, T) = \frac{G_F^2}{8\pi} [Z(4\sin^2\theta_W - 1) + N]^2 \times A \left(2 - \frac{TA}{E_\nu^2}\right) |f(q)|^2 \quad (1)$$

where  $A$ ,  $N$ , and  $Z$  are the mass number, number of neutrons, and number of protons in the nucleus, respectively. Further,  $E_\nu$  is the incident neutrino energy,  $T$  is nuclear recoil energy, with its maximum value denoted as ( $T_{\max}(E_\nu) = 2E_\nu^2/(A + 2E_\nu)$ ),  $G_F$  is the Fermi coupling constant,  $\theta_W$  is the weak mixing angle, and  $f(q)$  is the nuclear form factor for a momentum transfer  $q$ . For low-energy neutrinos ( $E_\nu < 50$  MeV), the momentum transfer is very small such that  $q^2R^2 < 1$ , where  $R$  is the radius of the nucleus,  $f(q) \sim 1$ . At small momentum transfers, the scattering amplitude from individual nucleons is in phase and added coherently, which leads to the increase of cross-section. The weak mixing angle  $\sin^2\theta_W$  has been experimentally determined to be  $0.23867 \pm 0.00016 \sim 1/4$  [43]. Hence, the cross-section is proportional to  $N^2$ . Although the scattering cross-section is enhanced by the number of nucleons, it depends on the measurement of very low energies of recoiling nuclei. The recoil energy of the nucleus depends on its mass, which decreases with the increase in the mass of target nuclei. For instance, with a neutrino energy of 1 MeV, the maximum recoil energy is about 20 eV and 50 eV for Ge and Si targets, respectively.

The maximal recoil energy of different target nuclei (Si, Ge) considered in this study is shown in Fig. 2 as a function of reactor  $\bar{\nu}_e$  energy. It can be observed from Eq. 1 that the cross-section is maximum at zero recoil energy and it decreases with the increase of  $T$ . Hence, a detector with a higher threshold energy for detecting the signal leads to a lesser number of events. Therefore, it is very tough to select the type of detector for the measurement of such a cross-section. Because of the low energy of the antineutrinos, the recoil energy deposited in the detector is up to a few keV.

#### V. EXPECTED EVENT RATE IN DETECTOR

The CE $\nu$ NS reaction cross section per unit detector mass could be up to two orders of magnitude greater than that for IBD process, potentially allowing for detectors in the kilogram range. The expected signal event rate due to CE $\nu$ NS is

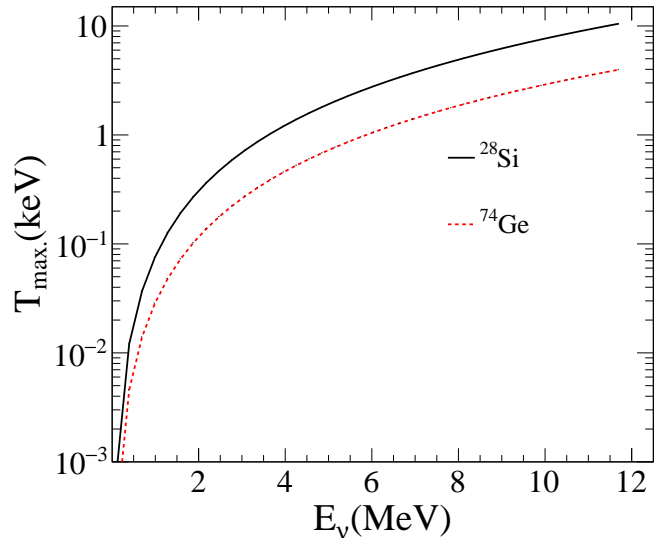


FIG. 2: Maximal recoil energy of Si and Ge nuclei as a function of energy of the reactor  $\bar{\nu}_e$ s.

given by

$$\frac{dN}{dT} = t\lambda_0 \frac{M_{\text{det}}}{A} \int_{E_\nu^{\min}}^{E_\nu^{\max}} \lambda(E_\nu) dE_\nu \int_{T_{\min}}^{T_{\max}} \left(\frac{d\sigma}{dT}(E_\nu)\right) dT(E_\nu), \quad (2)$$

where  $M_{\text{det}}$  is the mass of the detector,  $t$  is the time duration of data taking,  $\lambda_0$  is the total  $\bar{\nu}_e$  flux and,  $\lambda(E_\nu)$  is the  $\bar{\nu}_e$  energy spectrum. For a given experimental setup, the detector threshold decides the minimum recoil energy of the nuclei. Due to the lower abundance of  $\bar{\nu}_e$ s with energies exceeding 6.0 MeV, we have considered  $\bar{\nu}_e$ s with a maximum energy of approximately 6.0 MeV for the analysis. It can be noted here that the expected number of events in the detector is estimated by considering the contributions from each stable isotope of the element of the detector (Si or Ge) weighted by its natural abundance. Figure 3 shows the differential event rate dependence of maximal recoil energy for Ge and Si detectors. For a given recoil energy, the number of events increases with the target mass number due to an increase in the number of neutrons. However, the number of events decreases with the increase of recoil energy. Consequently, it becomes imperative to either augment the target mass or the energy of neutrinos for targets with lower mass numbers. As previously mentioned, the expected number of events also depends on the detector threshold. The number of events expected in the detector of mass 10 kg is mentioned in Table II. Events are estimated considering the detector is placed at 4m distance from the U-Apsara reactor core for an exposure of 1 year.

TABLE II: Expected events with different detectors placed at 4m from U-Apsara reactor

Threshold (eV)	Si detector	Ge detector
20.0	1443.0	2017.0
50.0	1256.0	1501.0
100.0	1038.0	982.0

## VI. NEUTRINO OSCILLATION PROBABILITY IN SHORT BASELINE EXPERIMENT

The CE $\nu$ NS process offers a distinct advantage in assessing ASN mixing sensitivity compared to the IBD process, owing to its higher cross-section. This allows for the use of smaller size detectors in CE $\nu$ NS measurements, thereby minimizing the uncertainty in the neutrino's path length. In the Standard Model, three active neutrino flavors ( $\nu_e, \nu_\mu, \nu_\tau$ ) are present, and their conversion to mass eigenstates is described by the Pontecorvo-Maki-Nakagawa-Sakata (PMNS) unitary matrix [44]. Numerous global efforts are underway to study neutrino oscillation phenomena and measure oscillation parameters for the three-generation model [45–53]. Beyond these, experiments are exploring to either find out or exclude the existence of sterile neutrinos, which has no analogous SM gauge interactions. However, its presence can affect the standard neutrino oscillations.

Firstly, a standard neutrino could oscillate into an undetectable sterile neutrino, leading to a reduction of the observed event rate within the detector. Secondly, the mass eigen-state ( $\nu_4$  with mass  $m_4$ ) primarily associated with the sterile neutrino would enhance the transformation probability between standard neutrinos, leading to the detection of a neutrino flavor that is not emitted by the source. The experiments looking for a reduction of the interaction rate are called “disappearance” experiments while the ones seeking an enhanced neutrino conversion are called “appearance” experiments.

In the context of ASN oscillation, the PMNS matrix extends to 3+1 from the standard 3 generations, with “3” representing active neutrinos and “1” representing a sterile neutrino ( $\nu_s$ ). The specifics of the rotation order and mixing matrix elements can be found in Ref. [54]. The 3+1 generation oscillation model reduced to a two-flavor framework for small mixing angles ( $\theta_{14}$ ) and short source-to-detector distances ( $< 100$  m). Then the  $\bar{\nu}_e$  survival probability can be approximated as

$$P_{\bar{\nu}_e\bar{\nu}_e}(E_\nu, L) \simeq 1 - \sin^2 2\theta_{14} \sin^2 \left( \frac{1.27\Delta m_{41}^2 L}{E_\nu} \right), \quad (3)$$

where  $E_\nu$  is the  $\bar{\nu}_e$  energy (in MeV),  $L$  is the path length (in m) between the source and the detector, and  $\Delta m_{41}^2$  is the squared masses difference (in eV<sup>2</sup>) between the two (anti)neutrino mass eigen-states. The ASN oscillation parameters  $\Delta m_{41}^2$  and  $\sin^2 2\theta_{14}$  are represented by

$$\Delta m_{41}^2 = m_4^2 - m_1^2; \quad \sin^2 2\theta_{14} = 4|U_{e4}|^2(1 - |U_{e4}|^2), \quad (4)$$

where  $U_{e4} = \sin \theta_{14}$ , one of the elements of unitary mixing matrix. The combined analysis of data obtained by NEOS

and DANSS collaborations provides the present best-fit values of ASN oscillation parameters as  $\Delta m_{41}^2 \simeq 1.30$  eV<sup>2</sup> and  $\sin^2 2\theta_{14} \simeq 0.049$  [55]. These findings align with the results of a global analysis [56]. With these values of ASN mixing parameters, experimentally, the possible existence of sterile neutrinos at short baseline can be observed by finding the distortions of the  $\bar{\nu}_e$  energy spectrum which is otherwise absent in three active neutrino oscillation.

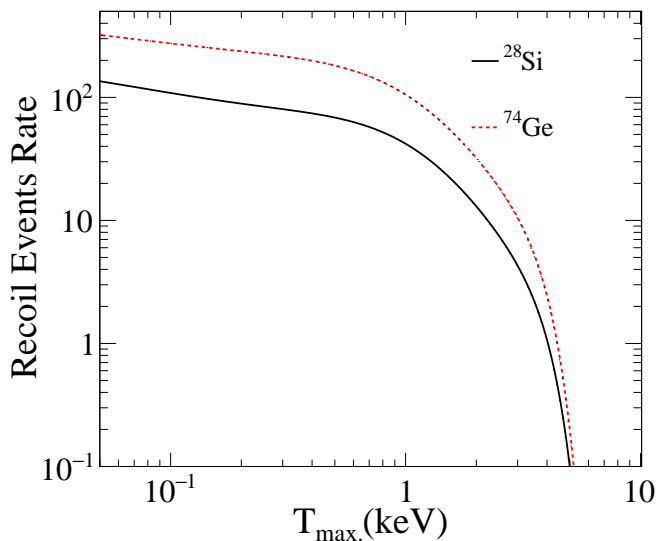


FIG. 3: Differential event rate variation with maximal recoil energy using Si and Ge detectors.

## VII. SIMULATION PROCEDURE

In the present study, the potential of different detectors has been explored for finding the ASN oscillation sensitivity by using the  $\bar{\nu}_e$ s produced from various types of reactor facilities as detailed in Table I. It is important to note that the energy spectrum of the  $\bar{\nu}_e$ s produced from these reactors varies across isotopes. Consequently, the number of  $\bar{\nu}_e$ s isn't solely dependent on thermal power but also on fuel compositions.

The spatial variation of  $\bar{\nu}_e$ s flux due to the finite-size cylindrical shape reactor core is considered which can be parameterized as [57],

$$\phi = \phi_0 J_0(2.405r/R) \cos(\pi z/H) \quad (5)$$

where  $\phi_0$  represents the flux at the center of the reactor core taken as the vertex position,  $R$ , and  $H$  are the physical radius and height of the cylindrical reactor core, respectively,

$J_0$  is the zeroth-order Bessel function of the first kind with  $r$  ( $0 \leq r \leq R$ ) and  $z$  ( $0 \leq z \leq H$ ). In this analysis, events are estimated using the reactor antineutrinos flux and CE $\nu$ NS cross-section, as previously outlined. The detector response to the recoil energy spectrum is incorporated by assuming a standard Gaussian form with the standard deviation( $\sigma$ ) for the energy resolution as given by

$$R^{\text{res}}(T_m, T) = \frac{1}{\sqrt{2\pi}\sigma} \exp\left(-\frac{(T_m - T)^2}{2\sigma^2}\right). \quad (6)$$

where  $T$  and  $T_m$  are the simulated true and observed recoil energy of nuclei, respectively. The detector resolution is considered as  $\sigma/T \sim 10\%/\sqrt{T}$ . The recoil energy spectrum generated due to  $\bar{\nu}_e$ s induced events is distributed with variable bin widths such that the minimum number of events in each bin is  $\geq 5$ . The number of events in  $i$ -th energy bin after folding the detector resolution is given as

$$N_i^r = \sum_k K_i^k (T^k) n_k \quad (7)$$

The index  $i$  corresponds to the measured energy bin and  $N_i^r$  represents the number of reconstructed events,  $k$  is summed over the true recoil energies of nuclei and  $n_k$  is the number of events in  $k$ -th true energy bin. Further,  $K_i^k$  is the integral of the detector resolution function over the  $T$  bins which is given as

$$K_i^k = \int_{T_{L_i}}^{T_{H_i}} dT \frac{1}{\sqrt{2\pi}\sigma_T^2} e^{-\frac{(T^k - T_m)^2}{2\sigma_T^2}} \quad (8)$$

The integration is performed between the lower and upper boundaries of the measured energy ( $T_{L_i}$  and  $T_{H_i}$ ) bins. In the present analysis, we have assumed 80% for the detection efficiency, 90% as the fiducial volume of the detector, and 70% reactor duty cycle for a total exposure of 1 year. The production points of  $\bar{\nu}_e$ s inside the reactor core are generated randomly using a Monte-Carlo method whereas a point detector is considered due to its compact size.

### VIII. EXTRACTION OF ACTIVE-STERILE NEUTRINO MIXING SENSITIVITY

The detector sensitivity to the ASN mixing can be extracted by knowing the neutrino energy spectrum, flux, and its cross-section accurately. A total number of neutrino-induced events expected within the detector can be estimated using the procedure mentioned above for a given oscillation hypothesis and it can be compared with the actual measured events. For this purpose, a statistical analysis between the predicted and expected event distribution by simulation is carried out in order to quantify the sensitivity of the detector to the ASN mixing parameters  $\theta_{14}$  and  $\Delta m_{41}^2$  for a given exposure. The detector response is folded in both simulation predicted as well as the expected events. The sensitivity to the sterile neutrino mixing parameters is extracted by estimating the  $\chi^2$  method. The

exclusion limit is obtained for each value of  $\Delta m_{41}^2$  by scanning over the various values of  $\sin^2 2\theta_{14}$  and identifying the boundary of the corresponding  $\chi^2$  (e.g.  $\chi^2 = 5.99$  for 95.0% confidence limit (C.L.)). The definition of  $\chi^2$  is taken from Ref. [58] and given as

$$\chi^2 = \sum_{n=0}^N \left( \frac{N_n^{\text{th}} - N_n^{\text{ex}}}{\sigma(N_n^{\text{ex}})} \right)^2 + \sum_{i=0}^k \xi_i^2, \quad (9)$$

where,  $n$  is the number of energy bins with variable widths,  $N_n^{\text{ex}}$ ,  $N_n^{\text{th}}$  are the number of events obtained from the simulations with oscillation (expected) and without oscillation (theoretically predicted) events, respectively. The theoretically predicted events  $N_n^{\text{th}}$  are calculated considering the reactor  $\bar{\nu}_e$  flux, the CE $\nu$ NS cross-section, detection efficiency, and energy resolutions of the detector as mentioned earlier. The  $N_n^{\text{ex}}$  is estimated by folding the oscillation probability on  $N_n^{\text{th}}$  along with the detector resolution. The  $N_n^{\text{th}}$  carries the information about the systematic uncertainties given by

$$N_n^{\text{th}} = N_n^{\prime\text{th}} \left( 1 + \sum_{i=0}^k \pi_n^i \xi_i \right) + \mathcal{O}(\xi^2) \quad (10)$$

with  $\pi_n^i$  being the strength of the coupling between the pull variable  $\xi_i$  and  $N_n^{\prime\text{th}}$ . The  $\chi^2$  is minimized with respect to pull variables  $\xi_i$  and it is estimated by considering four sources of systematic uncertainties. It includes 3.0% normalization uncertainty which arises due to reactor total neutrino flux, number of target atoms, and detector efficiency, uncertainty due to nonlinear energy response of the detector taken as 1.0%, and, uncertainty in the energy calibration given as 0.5%. In addition, the uncorrelated experimental bin-to-bin systematic error of 2.0% is also considered which could result due to the insufficient knowledge of other sources of background.

### IX. ACTIVE-STERILE NEUTRINO MIXING SENSITIVITY

Earlier, the sensitivity of ASN mixing was explored using the ISMRAN detector setup, assuming a fixed distance between the detector and the reactor core and  $\bar{\nu}_e$ s will be detected through the IBD process [42, 54]. The present analysis has been carried out by varying both the reactor and detector-related parameters with the neutrinos detected through CE $\nu$ NS process. The comparison of active to sterile neutrino oscillation parameters' sensitivity of various types of detectors is performed by employing  $\bar{\nu}_e$ s produced from different types of reactors as mentioned in Table I.

#### A. With Different Types of Detector

In contrast to the IBD scenario, there is a wider range of detector materials available in which CE $\nu$ NS can be measured. While the CE $\nu$ NS scattering cross section increases with the number of nucleons present in the target material, the recoil energy of the nuclei decreases with mass.

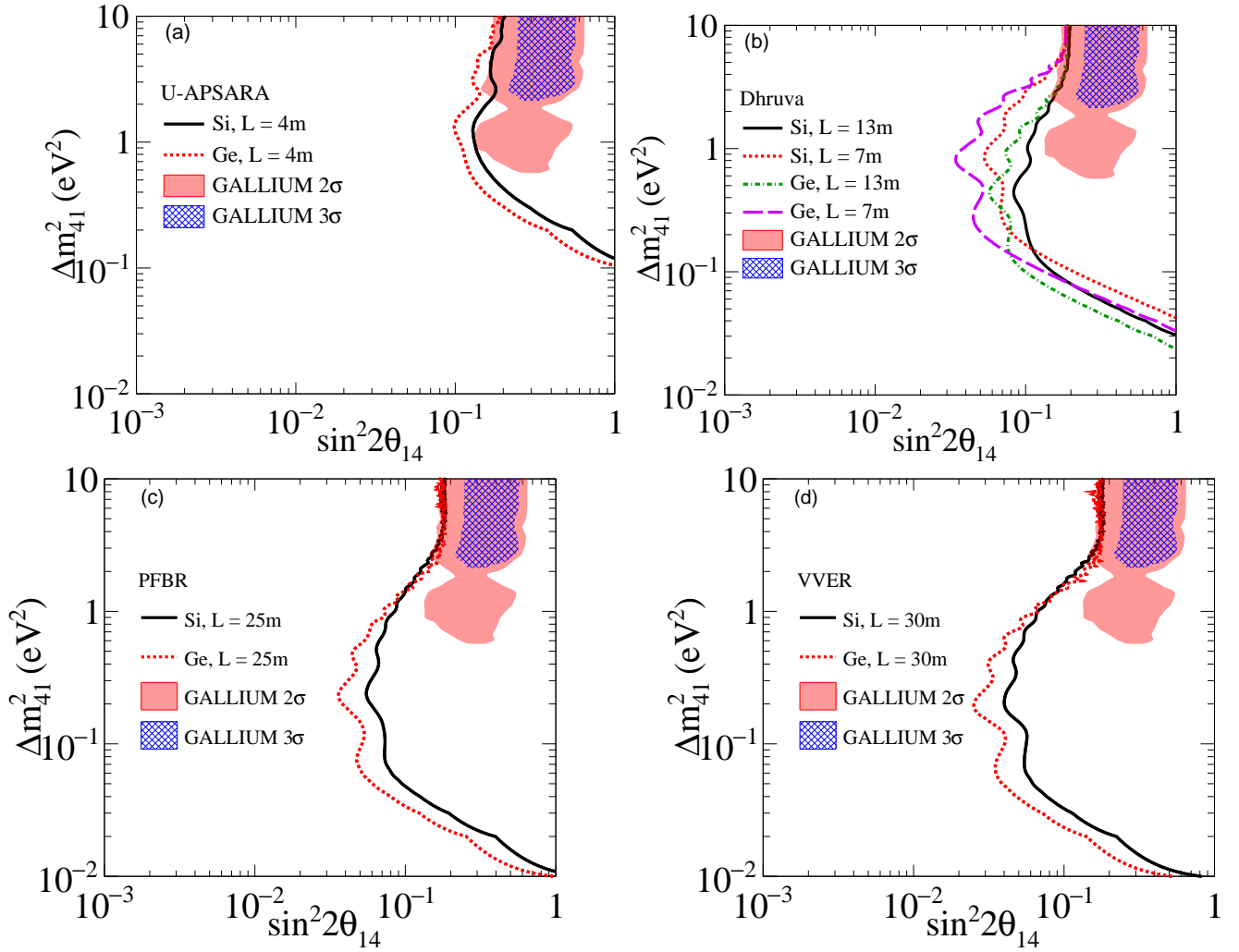


FIG. 4: The comparison of ASN mixing sensitivity at 95 % C.L. for the Ge and Si detectors placed at fixed distances of 4 m, 13 m, 25 m, and 30 m from the (a) U-Apsara, (b) DHRUVA, (c) PFBR and (d) VVER reactors, respectively.

The ASN mixing sensitivity of the detector has been studied considering commonly employed detector materials, such as Germanium (Ge) and Silicon (Si), each having a payload of 10 kg at a given reactor thermal power and reactor core to detector distance. Figure 4 shows the extracted results in  $\sin^2 2\theta_{14} - \Delta m_{41}^2$  plane at 95.0 % C.L. for an exposure of 1.0 year. Results are presented for different distances between the detector and the core of the reactor based on the accessibility conditions of different reactors. We assume a recoil energy threshold of 20.0 eV and 50.0 eV for Ge and Si detectors, respectively. Allowed regions for the Gallium anomaly are also depicted in the same figure [59]. Figure 4(a) shows the sensitivity by placing the detectors at 4 m from the U-Apsara research reactor core. Figure 4(b) shows the sensitivity of the detector by positioning it at 7.0 m and 13.0 m from the DHRUVA reactor core. Figure 4(c) shows the sensitivity of the detector at the PFBR reactor which is at a distance of 25.0 m from the detector, and Figure 4(d) shows the sensitivity for the detectors placed at 30 m from the VVER power reactor core. The shape of the sensitivity curve in the region of

low values  $\Delta m_{41}^2$  ( $\lesssim 1.0 \text{ eV}^2$ ) shows a linear dependence between  $\sin^2 2\theta_{14}$  and  $\Delta m_{41}^2$  in the logarithmic scale. This may happen as typical neutrino oscillation lengths are much larger as compared to the size of the detector, and the  $\bar{\nu}_e$  survival probability mentioned in Eq. 3 is approximately given by  $P_{\nu_e \nu_e}(E_\nu, L) \approx 1 - C \sin^2 2\theta_{14} \times (\Delta m_{41}^2)^2$ , where  $C$  is a constant. In the region with higher  $\Delta m_{41}^2$  values, the systematic uncertainties related to the neutrino source dominate over the statistical uncertainties. The detector energy resolution flattens the high frequency oscillation-induced deformations significantly, resulting in the gradual decrease of the shape-discriminating power. This leads to the event distribution, with and without oscillation, overlaps except for a constant normalization factor. It is also observed that, by placing the detector at a distance in the range of 15–30 m in the case of PFBR and VVER reactors, leads to a greater parts of the region can be excluded in the  $\sin^2 2\theta_{14} - \Delta m_{41}^2$  plane. Also, the maximum sensitivity of the detector shifts to a lower value of  $\Delta m_{41}^2$  ( $\sim 0.03 \text{ eV}^2$ ) due to the increase in source-to-detector

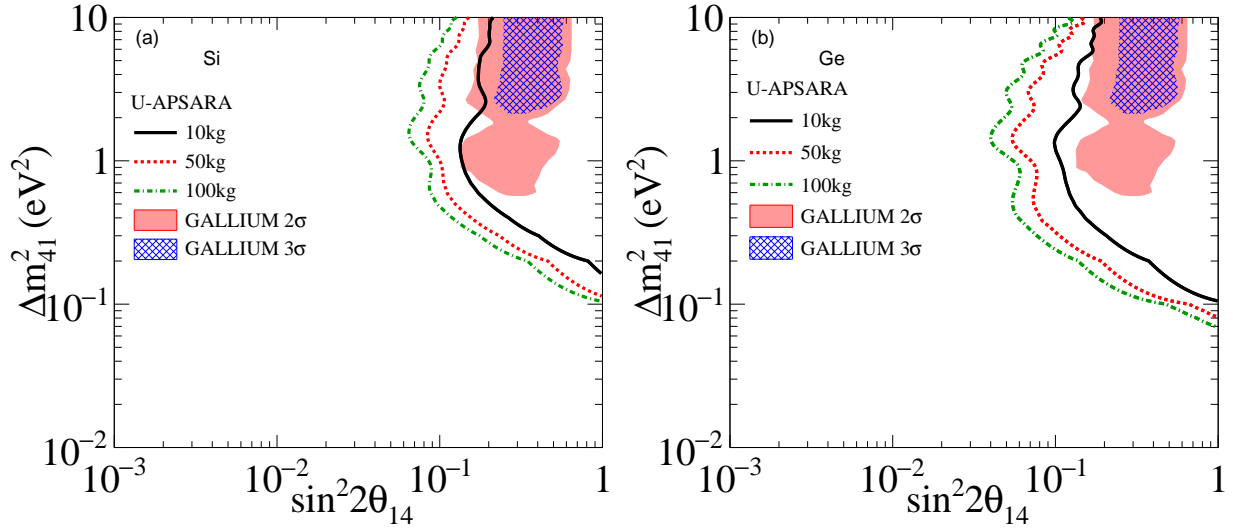


FIG. 5: The comparison of ASN mixing sensitivity at 95 % C.L. for different detector mass of the (a) Si and (b) Ge detectors placed at distance of 4 m from the U-Apsara reactor

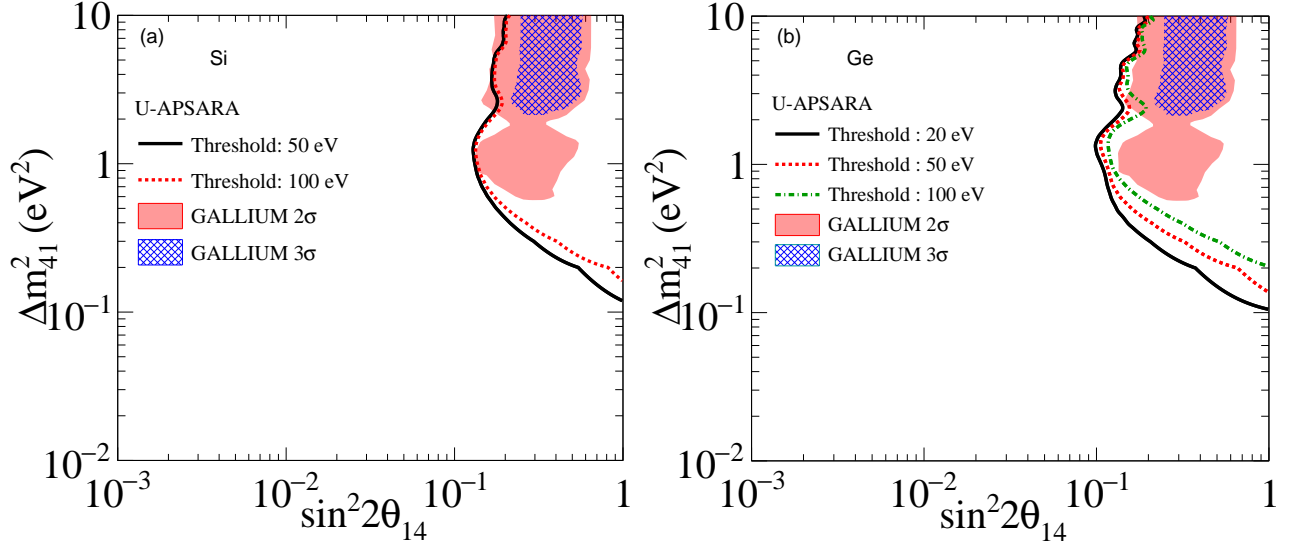


FIG. 6: The comparison of ASN mixing sensitivity at 95 % C.L. for different detector threshold for the (a) Si and (b) Ge detectors placed at 4 m from the U-Apsara reactor facility.

distance. Notably, the Ge detector demonstrates superior ASN mixing sensitivity compared to the Si detector when  $\Delta m_{41}^2$  is less than or equal to  $1.0 \text{ eV}^2$ . However, for higher values of  $\Delta m_{41}^2 > 1.0 \text{ eV}^2$ , both the detectors exhibit nearly identical sensitivity to the mixing angle  $\sin^2 2\theta_{14}$ . Both Si and Ge detectors exclude the allowed region of the GALLIUM experiment at C.L. of  $2\sigma$ . The detector sensitivity also depends on uncertainty in neutrino path length which occurs due to spatial variation of  $\bar{\nu}_e$ s flux and finite size of the detector. By smearing the  $\bar{\nu}_e$ s both vertex position in the reactor core (U-Apsara) and the detection position, it is observed that there is a maximum variation of about 2% in the mixing angle  $\sin^2 2\theta_{14}$  at  $\Delta m_{41}^2 > 5.0 \text{ eV}^2$  as compared to fixed path length. However, at lower  $\Delta m_{41}^2 (\leq 1.0 \text{ eV}^2)$ , there is a minimal effect to the

ASN oscillation parameters.

### B. With Different Masses of the Detector

The expected number of events decreases with a decrease in the target mass number. Therefore, to enhance the sensitivity of the detector, it is required to increase the neutrino flux, exposure time, or the target mass. At a given reactor power, in order to increase the CE $\nu$ NS interaction rate the actual target mass number of the detector is more crucial. Consequently, increasing the detector mass is a prudent choice, even if it adds some complexity to handling. Taking into account the backgrounds, it is observed that detectors in CE $\nu$ NS exper-



iment exhibit a mass advantage of one order of magnitude, assuming that measurements of eV-scale recoil thresholds are feasible and a signal-to-background ratio of about 1 can be achieved in the experiment [60]. Figure 5 shows the ASN mixing sensitivity in  $\sin^2 2\theta_{14} - \Delta m_{41}^2$  plane at 95% C.L. for an exposure of 1 yr for different mass of the detector. Figure 5(a) shows for Si detector and Fig. 5(b) for Ge detector, both with masses 10 kg, 50 kg, and 100 kg. It can be noted here that, sensitivities are extracted considering a threshold of 100 eV and 20 eV for silicon and germanium detector, respectively. At a given detector mass at higher  $\Delta m_{41}^2$  the sensitivity in  $\sin^2 2\theta_{14}$  is more as compared to lower  $\Delta m_{41}^2$ . The sensitivity improves in all regions of  $\sin^2 2\theta_{14}$  with an increase in detector mass as the number of expected events increases. It is evident that the Ge detector excludes both allowed regions of the GALLIUM experiment.

### C. With Various Detector Thresholds

As previously discussed, the recoil energy of nuclei decreases as the mass number of the detector increases. Therefore, detectors with low thresholds, such as Ge and Si can perform nuclear recoil discrimination down to the eV scale energy threshold. Such detectors will be more useful if we can observe the recoil energies as low as a few tens of eV. In the context of  $CE\nu NS$  cross-section, as given in Eq. 1, the nuclear recoil energy  $T$  serves as the relevant observable. For a given neutrino energy, there is a limit to the maximum recoil energy. The cross-section is maximum for lower values of  $T$ , therefore, the total number of observed event rate sensitivity dependent on the low-energy threshold for nuclear recoil  $T_{min}$ . A comprehensive study has been performed to assess the impact of detector threshold on ASN mixing sensitivity, considering both Si and Ge detectors with a mass of 10 kg placed at a distance of 4 m from U-Apsara reactor core. Figure 6 shows the sensitivity in  $\sin^2 2\theta_{14} - \Delta m_{41}^2$  plane at 95 % C.L for detector with different threshold energies. The sensitivity of the detector at lower  $\Delta m_{41}^2$  is better at the lower detector threshold. However, for  $\Delta m_{41}^2 \geq 1.0 \text{ eV}^2$ , the detector threshold has minimal impact on ASN mixing sensitivity.

### D. With Different Resolution of Detector

The sensitivity of the detector to the neutrino mixing parameters such as angle and squared mass difference depends on its resolution and efficiency. To investigate the effect of energy resolution, we have considered a 10 kg Ge detector positioned at a distance of 4m from the U-Apsara reactor core. The detector resolution varies from  $\sigma/E = 3\% - 10\%/\sqrt{E}$  for extracting its sensitivity to the upper limit for the ASN mixing angle  $\theta_{14}$ . Figure 7 shows the sensitivity to ASN mixing parameters in the  $\Delta m_{41}^2 - \sin^2 2\theta_{14}$  plane. It is observed that, the detector exhibits better sensitivity to the ASN mixing with a resolution of  $\sigma/E = 3\%/\sqrt{E}$ . Interestingly, for  $\Delta m_{41}^2 < 1.0 \text{ eV}^2$ , ASN mixing sensitivity remains unaffected by the detector resolution. However, for higher  $\Delta m_{41}^2 \geq 1.0 \text{ eV}^2$ , the

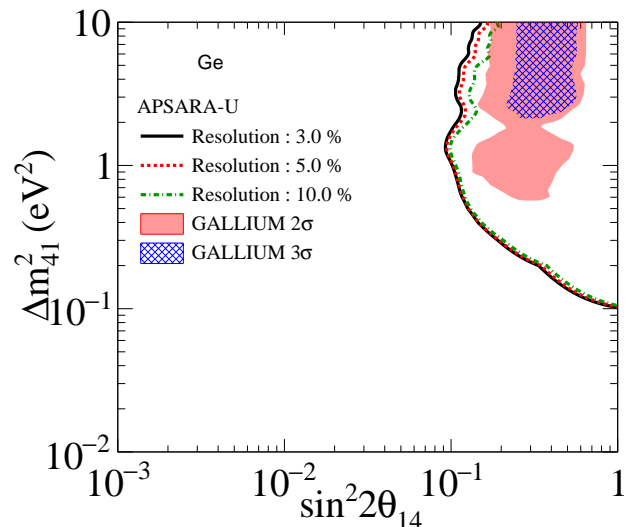


FIG. 7: The comparison of ASN mixing sensitivity at 95 % C.L. for different resolution of Ge detector placed at 4 m from the U-Apsara reactor facility.

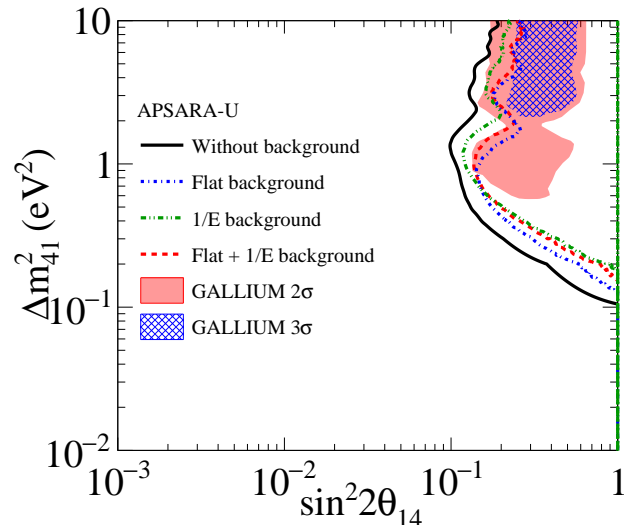


FIG. 8: The comparison of ASN mixing sensitivity at 95 % C.L. of Ge detector in presence of background placed at 4m from the U-Apsara reactor facility. The signal to background ratio is one considered here.

detector's resolution improves the ASN mixing sensitivity. At higher  $\Delta m_{41}^2$ , the oscillation frequency is more, and hence to have better sensitivity a detector with very good energy resolution is necessary.

### E. Sensitivity of Detector in Presence of Background

Measuring the low energy of recoil nuclei from the  $CE\nu NS$  process poses a significant challenge due to the presences of background. The background affects the detector sensitivity while extracting the various physics parameters of interest.

The ASN mixing sensitivity has been obtained by incorporating backgrounds, particularly in the context of Ge detector which will be placed in the above-ground conditions at 4.0m distance from U-Apsara reactor. At the experimental site, the reactor-related background (neutron and gamma) and cosmogenic background (muon-induced neutrons) that can not be eliminated even with the shielding and will contaminate the actual signal. It is not only the types of backgrounds but also the energy dependent shape of the background that affects the detector sensitivity. At low recoil energy, there are two types of background shapes such as  $1/T$  and flat-shaped backgrounds as mentioned in Ref. [60]. The simulated energy dependent background level due to neutron as well as gamma-rays are mentioned in Ref. [10]. In this study, the energy dependent background shape is considered from Ref. [60] with signal to background ratio of 1.0. While estimating the  $\chi^2$ , an associated 10% systematic uncertainty is therefore considered due to these backgrounds. Figure 8 shows the comparison of Ge detector sensitivity with and without the inclusion of backgrounds. It is observed that with the contribution of both backgrounds, the ASN mixing angle sensitivity is further reduced as compared to the case with no background. Therefore better background reduction techniques have to be employed for the measurement with required sensitivity.

## X. SUMMARY

The study on neutrinos provides avenues for exploring numerous phenomena in physics beyond the standard model. At

present, several experiments are underway to measure various fundamental properties of neutrinos emanating from different sources. A proposed experimental program at the U-Apsara research reactor, at BARC in India is described which aims to measure  $CE\nu NS$ . We have studied active-sterile neutrino mixing sensitivity with Si, and Ge detectors in the context of  $CE\nu NS$  measurements at reactors with different core configurations and sizes available in India. The analysis has been carried out to determine the active-sterile neutrino mixing sensitivity considering an exposure of 1 year and detectors with varying masses, detection thresholds, and resolutions. The region in  $\sin^2 2\theta_{14}-\Delta m_{41}^2$  plane is constrained by considering a single detector which will be placed at a fixed position with respect to the reactor core. It is found that the ASN oscillation at 95% confidence level with  $\sin^2 2\theta_{14} \geq 0.09$  at  $\Delta m_{41}^2 = 1.0 \text{ eV}^2$  can be observed with the Ge detector of mass 10 kg for an exposure of 1-yr. Additionally, the Ge detector can exclude a significant portion of the favored non-zero ASN mixing parameters region obtained from the GALLIUM experiment. Furthermore, the sensitivity improves when placing the detector at PFBR or VVER reactor facilities.

- 
- [1] F. An *et al.* (JUNO), *J. Phys. G* **43**, 030401 (2016), [arXiv:1507.05613 \[physics.ins-det\]](#) .
- [2] B. Abi *et al.* (DUNE), *Eur. Phys. J. C* **80**, 978 (2020), [arXiv:2006.16043 \[hep-ex\]](#) .
- [3] D. Z. Freedman, *Phys. Rev. D* **9**, 1389 (1974).
- [4] H. Bonet *et al.* (CONUS), *JHEP* **05**, 085 (2022), [arXiv:2110.02174 \[hep-ph\]](#) .
- [5] D. Akimov *et al.* (COHERENT), *Science* **357**, 1123 (2017), [arXiv:1708.01294 \[nucl-ex\]](#) .
- [6] E. Alfonso-Pita, L. J. Flores, E. Peinado, and E. Vázquez-Jáuregui, *Phys. Rev. D* **105**, 113005 (2022), [arXiv:2203.05982 \[hep-ph\]](#) .
- [7] J. Colaresi, J. I. Collar, T. W. Hossbach, C. M. Lewis, and K. M. Yocum, *Phys. Rev. Lett.* **129**, 211802 (2022), [arXiv:2202.09672 \[hep-ex\]](#) .
- [8] G. Agnolet *et al.* (MINER), *Nucl. Instrum. Meth. A* **853**, 53 (2017), [arXiv:1609.02066 \[physics.ins-det\]](#) .
- [9] D. Y. Akimov *et al.*, *JINST* **12**, C06018 (2017).
- [10] R. Strauss *et al.*, *Eur. Phys. J. C* **77**, 506 (2017), [arXiv:1704.04320 \[physics.ins-det\]](#) .
- [11] A. Aguilar-Arevalo *et al.* (CONNIE), *Phys. Rev. D* **100**, 092005 (2019), [arXiv:1906.02200 \[physics.ins-det\]](#) .
- [12] A. Aguilar-Arevalo *et al.* (CONNIE), *JHEP* **05**, 017 (2022), [arXiv:2110.13033 \[hep-ex\]](#) .
- [13] G. Fernandez-Moroni, P. A. N. Machado, I. Martinez-Soler, Y. F. Perez-Gonzalez, D. Rodrigues, and S. Rosauero-Alcaraz, *JHEP* **03**, 186 (2021), [arXiv:2009.10741 \[hep-ph\]](#) .
- [14] P. Coloma, M. C. Gonzalez-Garcia, M. Maltoni, and T. Schwetz, *Phys. Rev. D* **96**, 115007 (2017), [arXiv:1708.02899 \[hep-ph\]](#) .
- [15] J. Liao and D. Marfatia, *Phys. Lett. B* **775**, 54 (2017), [arXiv:1708.04255 \[hep-ph\]](#) .
- [16] M. Cadeddu, C. Giunti, Y. F. Li, and Y. Y. Zhang, *Phys. Rev. Lett.* **120**, 072501 (2018), [arXiv:1710.02730 \[hep-ph\]](#) .
- [17] T. S. Kosmas, O. G. Miranda, D. K. Papoulias, M. Tortola, and J. W. F. Valle, *Phys. Rev. D* **92**, 013011 (2015), [arXiv:1505.03202 \[hep-ph\]](#) .
- [18] B. C. Cañas, E. A. Garcés, O. G. Miranda, and A. Parada, *Phys. Lett. B* **784**, 159 (2018), [arXiv:1806.01310 \[hep-ph\]](#) .
- [19] D. K. Papoulias and T. S. Kosmas, *Phys. Rev. D* **97**, 033003 (2018), [arXiv:1711.09773 \[hep-ph\]](#) .
- [20] M. Biassoni and C. Martinez, *Astropart. Phys.* **36**, 151 (2012), [arXiv:1110.3536 \[astro-ph.HE\]](#) .
- [21] V. Brdar, M. Lindner, and X.-J. Xu, *JCAP* **04**, 025 (2018), [arXiv:1802.02577 \[hep-ph\]](#) .
- [22] G. Mention, M. Fechner, T. Lasserre, T. A. Mueller, D. Lhuillier, M. Cribier, and A. Letourneau, *Phys. Rev. D* **83**, 073006 (2011), [arXiv:1101.2755 \[hep-ex\]](#) .
- [23] T. A. Mueller *et al.*, *Phys. Rev. C* **83**, 054615 (2011), [arXiv:1101.2663 \[hep-ex\]](#) .
- [24] P. Huber, *Phys. Rev. C* **84**, 024617 (2011), [Erratum: *Phys.Rev.C* **85**, 029901 (2012)], [arXiv:1106.0687 \[hep-ph\]](#) .

- [25] F. P. An *et al.* (Daya Bay), *Phys. Rev. Lett.* **118**, 251801 (2017), [arXiv:1704.01082 \[hep-ex\]](#) .
- [26] G. Bak *et al.* (RENO), *Phys. Rev. Lett.* **122**, 232501 (2019), [arXiv:1806.00574 \[hep-ex\]](#) .
- [27] I. Alekseev *et al.* (DANSS), *Phys. Lett. B* **787**, 56 (2018), [arXiv:1804.04046 \[hep-ex\]](#) .
- [28] H. Almazán *et al.* (STEREO), *Phys. Rev. Lett.* **121**, 161801 (2018), [arXiv:1806.02096 \[hep-ex\]](#) .
- [29] J. Ashenfelter *et al.* (PROSPECT), *Phys. Rev. Lett.* **121**, 251802 (2018), [arXiv:1806.02784 \[hep-ex\]](#) .
- [30] A. P. Serebrov *et al.* (NEUTRINO-4), *Pisma Zh. Eksp. Teor. Fiz.* **109**, 209 (2019), [arXiv:1809.10561 \[hep-ex\]](#) .
- [31] A. Aguilar-Arevalo *et al.* (CONNIE), *JINST* **11**, P07024 (2016), [arXiv:1604.01343 \[physics.ins-det\]](#) .
- [32] D. Mulmule, S. P. Behera, P. K. Netrakanti, D. K. Mishra, V. K. S. Kashyap, V. Jha, L. M. Pant, B. K. Nayak, and A. Saxena, *Nucl. Instrum. Meth. A* **911**, 104 (2018), [arXiv:1806.04421 \[physics.ins-det\]](#) .
- [33] D. S. Akerib *et al.* (CDMS), *Phys. Rev. D* **72**, 052009 (2005), [arXiv:astro-ph/0507190](#) .
- [34] V. Sanglard *et al.* (EDELWEISS), *Phys. Rev. D* **71**, 122002 (2005), [arXiv:astro-ph/0503265](#) .
- [35] J. Liao, H. Liu, and D. Marfatia, *Phys. Rev. D* **108**, 033002 (2023), [arXiv:2302.10460 \[hep-ph\]](#) .
- [36] H. T. Wong *et al.* (TEXONO), *Phys. Rev. D* **75**, 012001 (2007), [arXiv:hep-ex/0605006](#) .
- [37] P. Vogel and J. Engel, *Phys. Rev. D* **39**, 3378 (1989).
- [38] T. Singh, P. Pandey, T. Mazumdar, K. Singh, and V. Raina, *Annals of Nuclear Energy* **60**, 141 (2013).
- [39] S. Agarwal, C. Karhadkar, A. Zope, and K. Singh, *Nuclear Engineering and Design* **236**, 747 (2006), india's Reactors: Past, Present, Future.
- [40] S. Chetal, V. Balasubramanian, P. Chellapandi, P. Mohanakrishnan, P. Puthiyavinayagam, C. Pillai, S. Raghupathy, T. Shanmugham, and C. S. Pillai, *Nuclear Engineering and Design* **236**, 852 (2006), india's Reactors: Past, Present, Future.
- [41] S. Agrawal, A. Chauhan, and A. Mishra, *Nuclear Engineering and Design* **236**, 812 (2006), india's Reactors: Past, Present, Future.
- [42] S. P. Behera, D. K. Mishra, and L. M. Pant, *Phys. Rev. D* **102**, 013002 (2020), [arXiv:2007.00392 \[hep-ph\]](#) .
- [43] J. Erler and M. J. Ramsey-Musolf, *Phys. Rev. D* **72**, 073003 (2005), [arXiv:hep-ph/0409169](#) .
- [44] Z. Maki, M. Nakagawa, and S. Sakata, *Prog. Theor. Phys.* **28**, 870 (1962).
- [45] R. Wendell *et al.* (Super-Kamiokande), *Phys. Rev. D* **81**, 092004 (2010), [arXiv:1002.3471 \[hep-ex\]](#) .
- [46] B. Aharmim *et al.* (SNO), *Phys. Rev. C* **88**, 025501 (2013), [arXiv:1109.0763 \[nucl-ex\]](#) .
- [47] S. Abe *et al.* (KamLAND), *Phys. Rev. Lett.* **100**, 221803 (2008), [arXiv:0801.4589 \[hep-ex\]](#) .
- [48] F. P. An *et al.* (Daya Bay), *Phys. Rev. Lett.* **108**, 171803 (2012), [arXiv:1203.1669 \[hep-ex\]](#) .
- [49] J. K. Ahn *et al.* (RENO), *Phys. Rev. Lett.* **108**, 191802 (2012), [arXiv:1204.0626 \[hep-ex\]](#) .
- [50] Y. Abe *et al.* (Double Chooz), *Phys. Rev. D* **86**, 052008 (2012), [arXiv:1207.6632 \[hep-ex\]](#) .
- [51] M. H. Ahn *et al.* (K2K), *Phys. Rev. D* **74**, 072003 (2006), [arXiv:hep-ex/0606032](#) .
- [52] P. Adamson *et al.* (MINOS), *Phys. Rev. D* **86**, 052007 (2012), [arXiv:1208.2915 \[hep-ex\]](#) .
- [53] K. Abe *et al.* (T2K), *Nucl. Instrum. Meth. A* **659**, 106 (2011), [arXiv:1106.1238 \[physics.ins-det\]](#) .
- [54] S. P. Behera, D. K. Mishra, and L. M. Pant, *Eur. Phys. J. C* **79**, 86 (2019), [arXiv:1901.04746 \[hep-ph\]](#) .
- [55] S. Gariazzo, C. Giunti, M. Laveder, and Y. F. Li, *Phys. Lett. B* **782**, 13 (2018), [arXiv:1801.06467 \[hep-ph\]](#) .
- [56] M. Dentler, A. Hernández-Cabezudo, J. Kopp, P. A. N. Machado, M. Maltoni, I. Martinez-Soler, and T. Schwetz, *JHEP* **08**, 010 (2018), [arXiv:1803.10661 \[hep-ph\]](#) .
- [57] S. Glasstone and A. Sesonske, *Reactor Syst. Eng.* **2**, 506 (1994).
- [58] M. C. Gonzalez-Garcia and M. Maltoni, *Phys. Rev. D* **70**, 033010 (2004), [arXiv:hep-ph/0404085](#) .
- [59] J. Kopp, P. A. N. Machado, M. Maltoni, and T. Schwetz, *JHEP* **05**, 050 (2013), [arXiv:1303.3011 \[hep-ph\]](#) .
- [60] M. Bowen and P. Huber, *Phys. Rev. D* **102**, 053008 (2020), [arXiv:2005.10907 \[physics.ins-det\]](#) .